Copyright Warning & Restrictions

The copyright law of the United States (Title 17, United States Code) governs the making of photocopies or other reproductions of copyrighted material.

Under certain conditions specified in the law, libraries and archives are authorized to furnish a photocopy or other reproduction. One of these specified conditions is that the photocopy or reproduction is not to be "used for any purpose other than private study, scholarship, or research." If a, user makes a request for, or later uses, a photocopy or reproduction for purposes in excess of "fair use" that user may be liable for copyright infringement,

This institution reserves the right to refuse to accept a copying order if, in its judgment, fulfillment of the order would involve violation of copyright law.

Please Note: The author retains the copyright while the New Jersey Institute of Technology reserves the right to distribute this thesis or dissertation

Printing note: If you do not wish to print this page, then select "Pages from: first page # to: last page #" on the print dialog screen

ABSTRACT

Subthreshold Channel Leakage Current in GaAs MESFET's

by
WEI LONG

In this thesis, a physical model including the subthreshold conpensation properties is presented. The Poisson equation is solved analytically in one dimension for GaAs MESFET's with undoped substrates in the subthreshold region. The solution is then used to derive expressions for subthreshold drain current and subshreshold swing in MESFET's with undoped substrates. Very good agreement between experimental and analytical results is achieved.

Two key parameters (Mo and Iso) that determine the subthreshold Characteristics have been analyzed as a function of residual acceptor concentration Na, deep level EL2 concentration Nt, channel doping concentration Nd and threshold voltage Vt. It is shown that Mo increases with Na and Nt increase, but decreases with Nd and Vt increase. For Iso, the results show it increase with Nd, Nt and Vt increase, but decreases with Na increases. The results also show that Nt has much smaller effect on subthreshold characteristics than Nd, Na and Vt. According to the results, very useful design rules are presented for the design of devices with good subthreshold leakage characteristics.

In addition to providing quick evaluation expressions, the analytical model presented in this thesis also gives us simple explanation for the observed subthreshold characteristics and offering a useful basis for accurate analysis, simulation and fabrication of GaAs FET's with ultra low leakage current.

SUBTHRESHOLD CHANNEL LEAKAGE CURRENT IN GAAS MESFET'S

by
Wei Long

A Thesis
Submitted to the Faculty of
New Jersey Institute of Technology
in Partial Fulfillment of the Requirments of the Degree of
Master of Science in Applied Physics

Department of Physics

October 1994

APPROVAL PAGE

SUBTHRESHOLD CHANNEL LEAKAGE CURRENT IN GaAs MESFET's

Wei Long

Dr. Ken K. Chin, Thesis Advisor — Date
Professor of Physics, NJIT

Dr. K. R. Farmer, Committee Member — Date
Assistant Professor in Applied Physics, NJIT

Dr. G. H. Feng, Committee Member — Date
Visiting Research Professor in Applied Physics, NJIT
Senior Research Scientist, Applied Optronics, South Plainfield, NJ

BIOGRAPHICAL SKETCH

Author: Wei Long

Degree: Master of Science in Applied Physics

Date: October 1994

Undergraduate and Graduate Education:

- Master of Science in Applied Physics,
  New Jersey Institute of Technology, Newark, NJ, 1994
- Master of Science in Electrical Engineering
  Shanghai Institute of Metallurgy, Academia Sinica, Shanghai, China
- Bachelor of Engineering in Electrical Engineering
  Tsinghua University, Beijing, China, 1983

Major: Applied Physics

This thesis is dedicated to
my mother

ACKNOWLEDGMENT

The author wishes to express his sincere gratitude to his advisor, professor Ken K. Chin, for his valuable inspiration , encouragement , guidance and support throughout the whole period of this MS study, without which it would not have been completed.

The author is grateful to Dr. K. R. Farmer and Dr. G. H. Feng for their resourceful suggestions and help.

Further , the author appreciates the timely help and suggestions from the group members.

Special thanks to his wife W. L. Yu who encourage him so much during his study in the United States.

Finally , the author likes to thank all his friends in NJIT for their kindness and help.

TABLE OF CONTENTS

LIST OF FIGURES

Figure Page

CHAPTER 1

INTRODUCTION

1.1 Significance of Leakage Current Research

The 8-12μ atomspheric window Long Wavelength Infrared (LWIR) photodetection by intersubband absorption in multiple quantum wells (MQW) or superlattices has recently become the subject of extensive investigation utilizing the GaAs/AlGaAs system[1], and efforts have been made to realize the possibility of potential monolithic integration of GaAs/AlGaAs MQW photodetectors with GaAs MESFET's (Metal Semiconductor Field Effect Transistors) electronics. GaAs FET devices with subthreshold leakage currents lower than 10^{-12} A are required in order to operate very weak photo-currents, which are typically in the $10^{-10}-10^{-12}$A range. One of the main reasons for the lack of progress in the development of monolithically integrated GaAs/AlGaAs superlattice devices, such as 8-12μ image sensors or focal plane arrays (FPA), is the extremely stringent requirment on the GaAs FET devices incorporated in such an OEIC (Opto-Electronics Integrated Circuit)

Most present-day GaAs integrated circuits are fabricated by making active regions on semi-insulating (SI) substrates grown by the liquid encapsulated Czochralski (LEC) technique. Unlike silicon technologies, device isolation is achieved by utilizing the high resistivity (about $10^{17}\Omega\cdot$cm at 300°K) of the bulk substrate material (Figure 1.1). Accompanying this structure is its special subthreshold characteristics. If the devices are not properly designed and carefully fabricated the subthreshold leakage current may become comparable with the weak signal current and hence cause serious problems. So accurate modeling of the

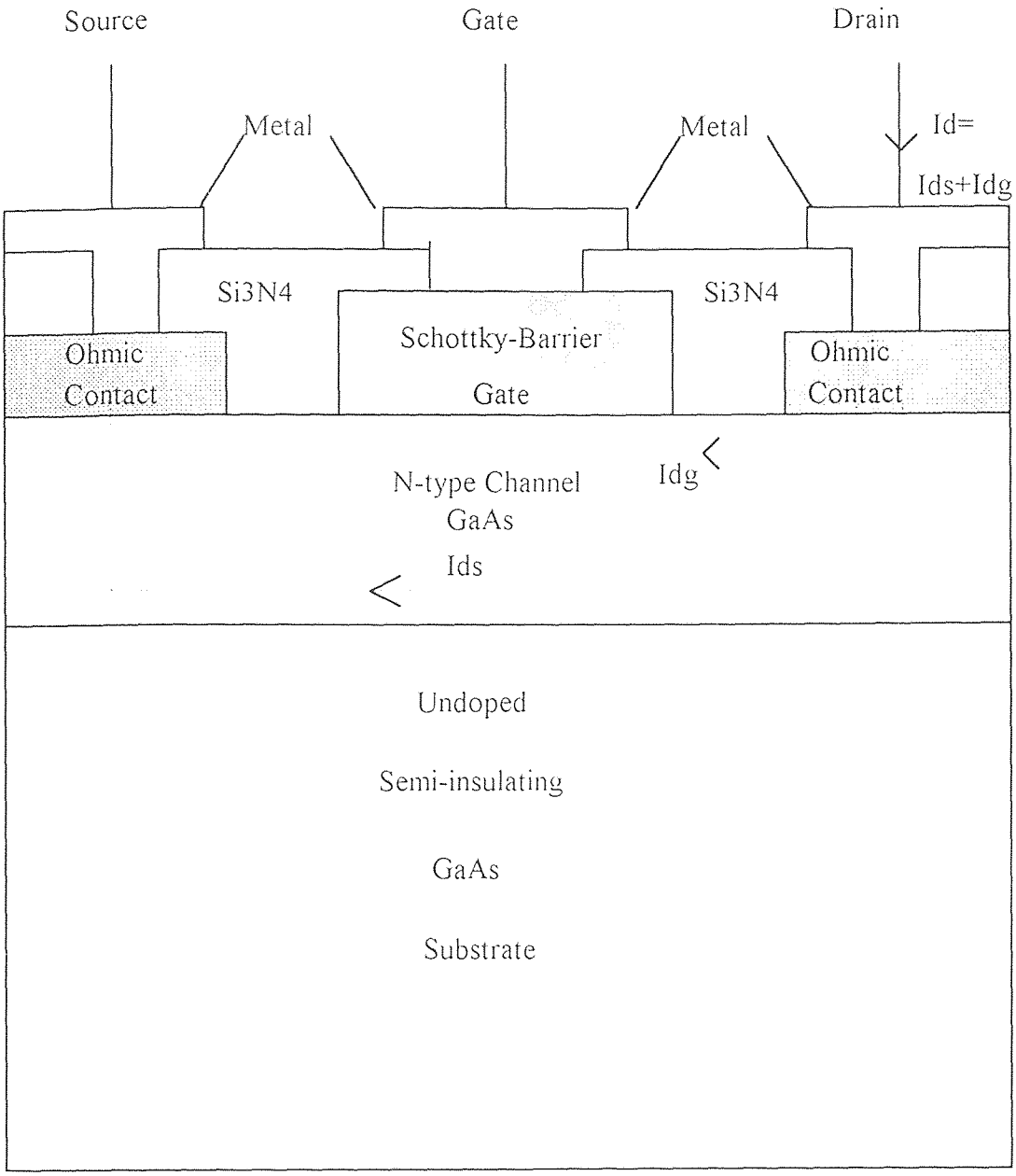

Figure 1.1 Typical GaAs MESFET Structure

subthreshold region of operation becomes increasingly important for the device and circuit design of monolithic GaAs photodetector.

1.2 The Objective of This Thesis

The subthreshold leakage current may go through bulk and the surface. Since the surface leakage current is processing dependent, in a well-controlled device process, the surface leakage current is negligible. Thus the aim of this work is to investigate the properties of subthreshold characteristics of MESFET's, i.e., bulk leakage. The bulk leakage current I_d may have two main components, I_{ds} and I_{dg}, as shown in Figure 1.1, where I_{ds} is the channel leakage current and I_{dg} is the gate Schottky diode reverse bias leakage current. In this thesis the main issue is about the subthreshold characteristics of I_{ds} and the behavior of I_{dg} is also discussed. Initially, A physical model is presented to derive the expressions for subthreshold leakage current. The Poisson equation is solved analytically in one dimension for MESFET's with undoped substrates. On the basis of these results, expressions for subthreshold drain current and subthreshold swing in MESFET's with undoped substrates are derived. These expressions are compared with practical MESFET data. The dependence of substrate properties and device parameters on the subthreshold channel leakage current is discussed. Simple explanations for observed data were provided.

CHAPTER 2

PHYSICAL MODEL

2.1 Deep Energy Level EL2

The development of GaAs integrated circuits needs a reliable supply of semi-insulating substrates with reproducible and thermally stable properties suitable for device fabrication. The liquid encapsulated Czochralski (LEC) technique is receiving considerable attention , because semi-insulating material can be grown without intentional doping and the technique offers the potential for producing round, large-area substrates with uniform properties at a reasonable cost. It has been well established that the semi-insulating properties of undoped bulk LEC GaAs result from the compensation of shallow acceptor impurities by deep EL2 (Energy Level 2) donors[2]. To account for this phenomenon in the derivation, Shockley-Read-Hall statistics are applied to the deep EL2 level[3]. As a result, the ionized deep donor concentration N_t^+ is given by (see figure 2.1)

$$N_t^+ = \frac{e_n + c_n P}{e_n + e_p + c_n n + c_p P} N_t \qquad (2.1)$$

where e_n is the electron emission coefficient of deep level , c_n the electron capture coefficient of deep level , e_p the hole emission coefficient of the deep level, c_p the hole capture coefficient of the deep level, N_t the conduction band effective density of states, n the electron concentration and p the hole concentration.

Various experiments also show that the EL2 level is an electron trap, i.e. , the value of the hole capture cross section (about $2 \cdot 10^{-18} cm^{-2}$) of this level is much smaller than the electron capture cross section (about $10^{-16} cm^{-2}$)[4]. Hence the

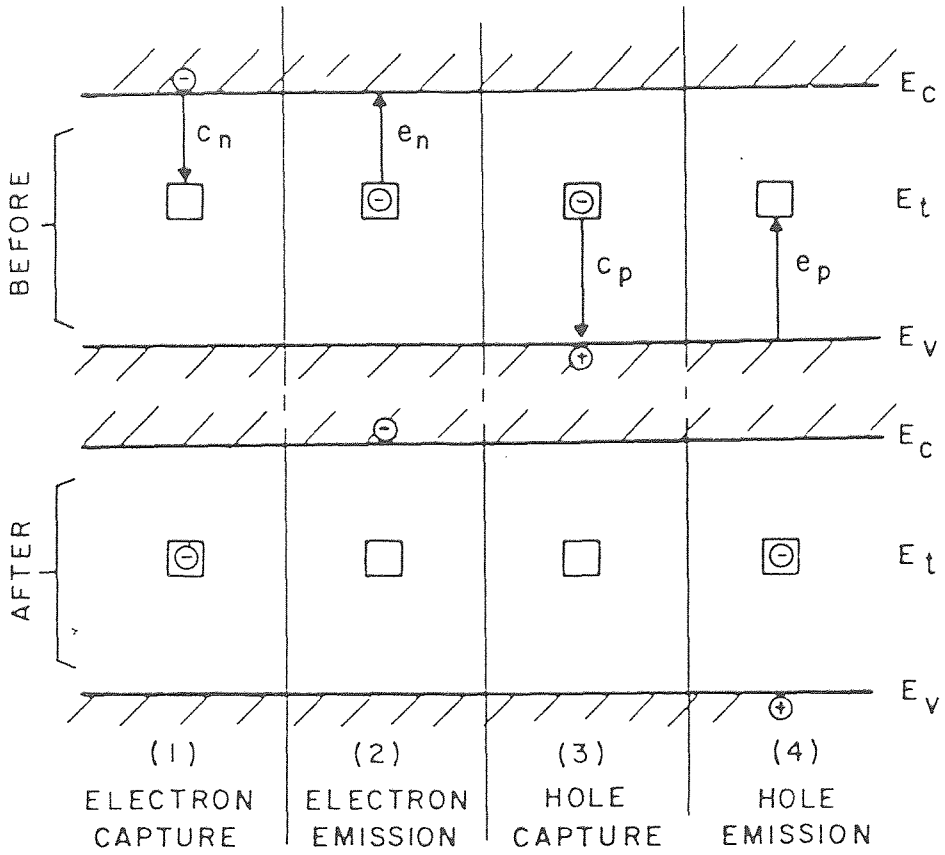

Figure 2.1 Deep energy level (EL2) recombination process

above equation can be further simplified by neglecting the hole capture and emission terms. Furthermore, the hole capture coefficient is related to the emission coefficient by[3]

$$\frac{e_n}{c_n} = n\, e^{[(E_t - E_f)/KT]} = N_c\, e^{[(E_t - E_c)/KT]} \qquad (2.2)$$

where E_t is the EL2 energy-level related to the conduction band, N_c the effective

density states in conduction band, E_f the Fermi energy level and E_c the conduction band energy level.

By substituting this relation into (2.1), the ionized deep-trap concentration becomes

$$N_t^+ = \frac{N_c\, e^{[-(E_c - E_t)/KT]}}{n + N_c\, e^{[-(E_c - E_t)/KT]}} \tag{2.3}$$

2.2 Basic Equations

For majority-carrier semiconductor devices in dc steady state, the basic equations that govern the behavior of devices are given by the following:

Poisson's equation :

$$\nabla \cdot (-\varepsilon \nabla \psi) = -\rho/\varepsilon \tag{2.4}$$

Electron current continuity equation ignoring electron generation and recombination:

$$(1/q)\nabla \cdot \mathbf{J}_n = 0 \tag{2.5}$$

Current density equation:

$$J_n = q\,\mu_n\, n\, E + qD_n \nabla n \tag{2.6}$$

Here ψ is the potential corresponding to the conduction-band energy, ρ the charge density, ε the GaAs dielectric constant, q the electron charge , $\mathbf{J}_n$ the electron current density, μ_n the electron mobility, $\mathbf{E}$ the electric field density and D_n the electron diffusion constant.

Since a semi-insulating substrate contains shallow acceptors(residual carbon) and deep donors (EL2), in this model, the charge density in (1.4) is given by

$$\rho = q\,(\,N_d^+ - N_a^- + N_t^+ - n + p) \tag{2.7}$$

With n and p are expressed as

$$\rho = n_i \, e^{[q(\psi - \psi_n)/KT]} \tag{2.8}$$

$$\rho = n_i \, e^{[q(\psi - \psi_p)/KT]} \tag{2.9}$$

Where N_d^+ is the concentration of ionized shallow donors in the active layer, N_a^- and N_t^+ are the concentration of ionized shallow acceptors and deep donors in the semi-insulating substrate, n and p are the electron and hole concentrations and ψ_n and ψ_p the hole quasi-Fermi potentials.

In the above equations, it is assumed that the electron is the majority carrier.

The electron mobility is modeled by the following expression:

$$\mu = \mu_0 \frac{1 + (v_s / \mu_0)(E / E_c)^4}{1 + (E / E_c)^4} \tag{2.10}$$

Where the low-field mobility $\mu_0 = 4500 cm^2/V \cdot s$, critical electric field Ec=4000 V/cm, and saturation velocity $v_s = 0.85 \times 10^7$ cm/s [5].

CHAPTER 3

CHARACTERISTICS OF THE JUNCTION OF AN N-TYPE ACTIVE LAYER AND A SEMI-INSULATING SUBSTRATE

3.1 Physics in the n - SI Junction

In order to derive the expression for MESFET's drain current in the subthreshold region, we need to know the built-in potential and the corresponding depletion width and charge densities of an n-SI (semi-insulating) junction. We need also to know the behavior of the n-SI junction. Consider an n-type GaAs layer found on top of a semi-insulating substrate. In thermal equilibrium, the Fermi level is constant throughout the system. Because of the impurity concentration gradient, there exists a potential barrier between the n-layer and the semi-insulating layer (see Figure 3.1). The positive charges needed to support the barrier come from ionized donor impurities (N_d^+) in the n-layer space-charge region near the junction. The negative charges, one might believe, arise from the mobile electrons on the semi-insulating side which shows n^- characteristics. (Similar to the situation in an n-n^- junction). However , the situation here is different. As shown in Figure 3.1 , in the space-charge region on the semi-insulating side, the deep donor levels are well below the Fermi energy level, thus they are occupied by electrons and are in a charge-neutral state. As a result, negative charges of residual ionized shallow acceptor impurities (N_a) are exposed and thus contribute to establishing the potential barrier. As the bulk substrate region is approached, the deep donor levels are closer to the Fermi level and part of them are ionized to $EL2^+$ and compensate the shallow acceptors. So the space charge region is very similar to the general depletion region.

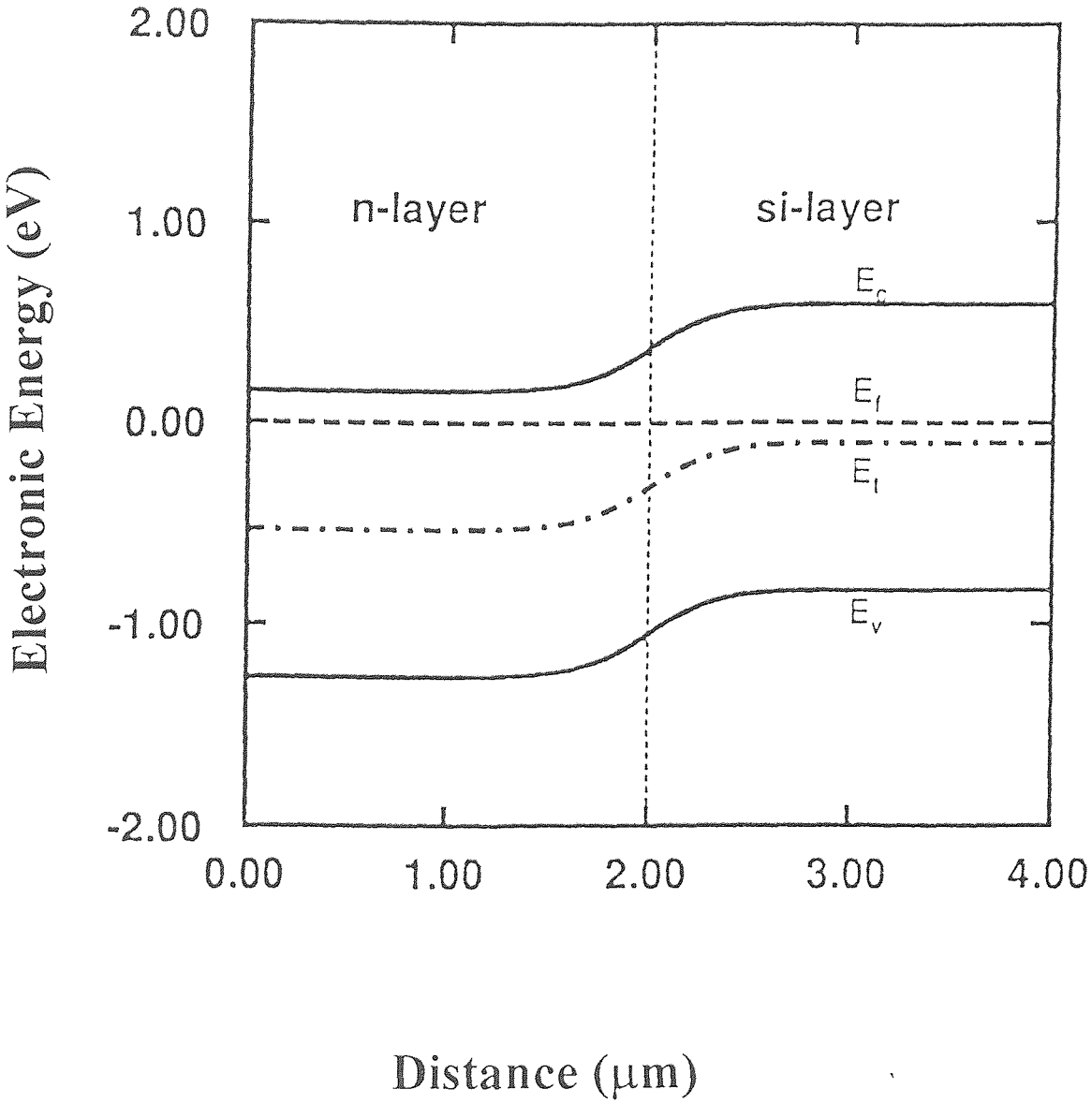

Figure 3.1 The band structure of an n-SI junction. The dashed line indicates the junction plane

3.2 Comparison with Conventional n-p Junction

From the above discussion, the behavior of an n-SI structure near the junction region is somewhat similar to that of an n-p junction with the p side doped with a concentration equal to that of the residual acceptor concentration in the SI-layer. However, there is a major difference between these two structures; the height of the potential barrier is different. In a semiconductor n-p junction, the built-in potential barrier height is given by[6]

$$V_{bi}(n-p) = \frac{KT}{q} \ln\left(\frac{N_d N_a}{n_i^2}\right) \tag{3.1}$$

On the other hand, the built-in potential in an n-SI junction is given by

$$V_{bi}(n\text{-}SI) = \frac{KT}{q} \ln\left[\frac{N_d}{n(SI)}\right] \tag{3.2}$$

where N_d is donor concentration on the n side and n(SI) is the equilibrium electron concentration in the semi-insulating region.

3.3 The Quantity n(SI) and Built-in Potential

The quantity n(SI) can be evaluated from the charge neutrality requirement which prevails in the neutral semi-insulating region

$$N_t^+ - N_a + p - n = 0 \tag{3.3}$$

Where N_a represents the residual acceptor concentration and N_t^+ is given by equation (2.3). In writing this expression, we assume that the residual donor concentration is smaller than the residual acceptor concentration in the semi-insulating material, which is a required condition for producing semi-insulating properties by involving deep donor levels [7]. Since the material is semi-insulating, the free carrier concentrations n and p are several orders of magnitude smaller than the other impurity quantities. By neglecting the free carrier concentration terms

and by substituting (2.3) for the ionized deep-donor concentration, the equilibrium electron concentration in the neutral semi-insulating substrate is estimated to be

$$n(SI) = (\frac{N_t}{N_a} - 1)N_c \exp[-(E_c - E_t)/KT] \tag{3.4}$$

By substituting this equation into (3.2) , the built-in potential becomes

$$V_{bi}\ (n\text{-}SI) = \frac{KT}{q} \ln[\frac{N_d N_a}{(N_t - N_a) N_c}] + \frac{E_c - E_t}{q} \tag{3.5}$$

Thus the potential barrier height in an n-SI junction is determined by the energy level of the deep donor and is smaller than that of the corresponding n-p junction. This is demonstrated in Figure 3.2. In all the calculations , the deep donor energy level in the SI material is assumed to be at an energy level of 0.69 eV below the conduction band and with a concentration of 10^{16} cm^{-3}. The residual acceptor concentration on the semi-insulating side and the donor concentrations on the n side both are assumed to be equal to 10^{15} cm^{-3}. The difference between the two barrier heights is seen to be about 0.58 eV.

3.4 Modeling of n-SI Junction

With the n-p junction forward-biased by the amount 0.58 V which is equal to the difference of the barrier heights of the two junction types in thermal equilibrium, the net charge distributions are shown in Fig. 3.3. While in the n-p junction the negative charges come from the ionized acceptors (solid line in Fig.3.3), the difference in the shallow acceptor (N_a) and deep donor concentrations (N_t^+) gives the same result for the n-SI junction. Although the origins of the charges are different , the net effects are the same in both cases. The resulting band diagrams are indistinguishable from each other. Therefore, if the tiny amount of the current flow in the slightly forward-biased n-p junction is neglected, the n-SI junction can be modeled by the equivalent forward-biased n-p junction with the doping

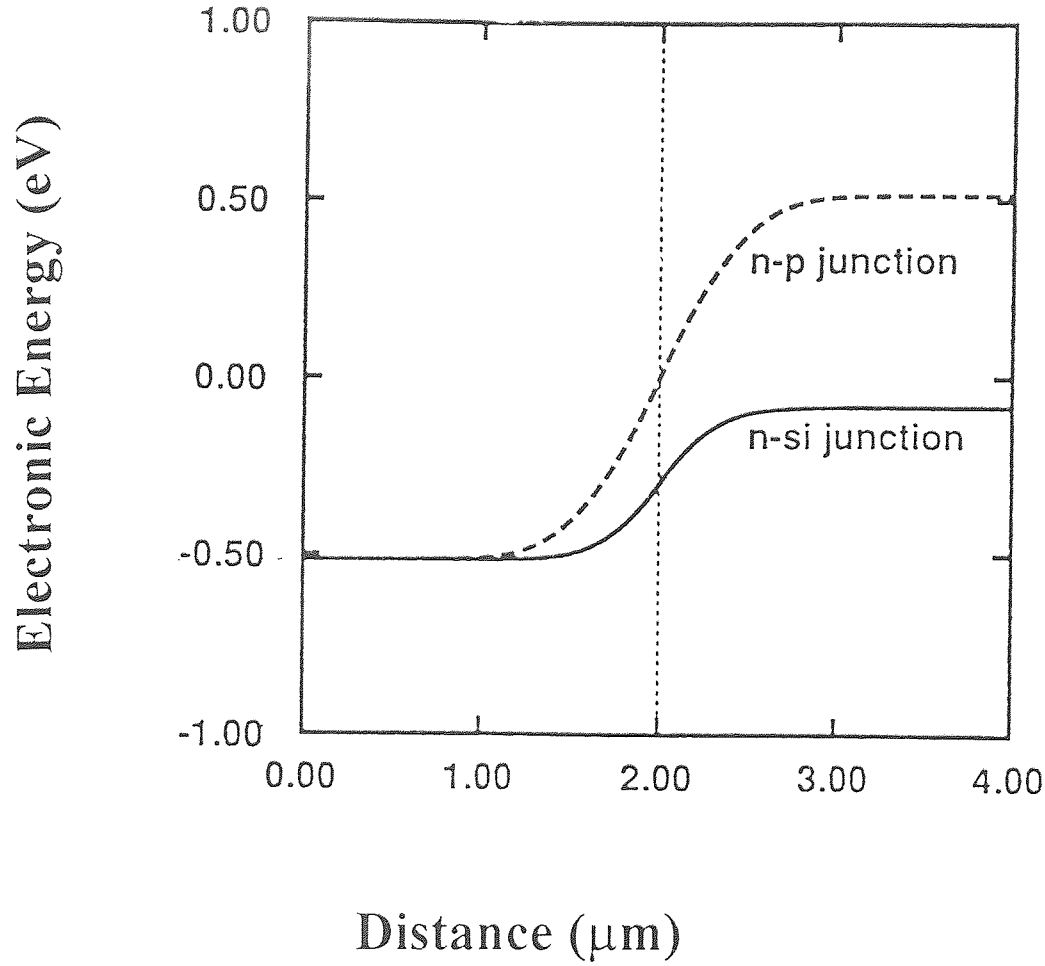

Figure 3.2 Comparison of calculated results of n-si (solid line) and corresponding n-p (thick dashed line) junctions. Both junctions are in thermal equilibrium. The junction plane is indicated by the vertical thin dash line at 2 μm.

concentration in the p-type material equal to that of the residual acceptor concentration(N_a) in the semi-insulating material and with the forward-biased voltage equal to the potential height difference. Therefore, the relationship between the depletion width and the potential barrier derived for n-p junction can be applied to n-SI junction by using the residual acceptor concentration on the semi-insulating layer and by taking into account of the built-in potential of the n-SI junction.

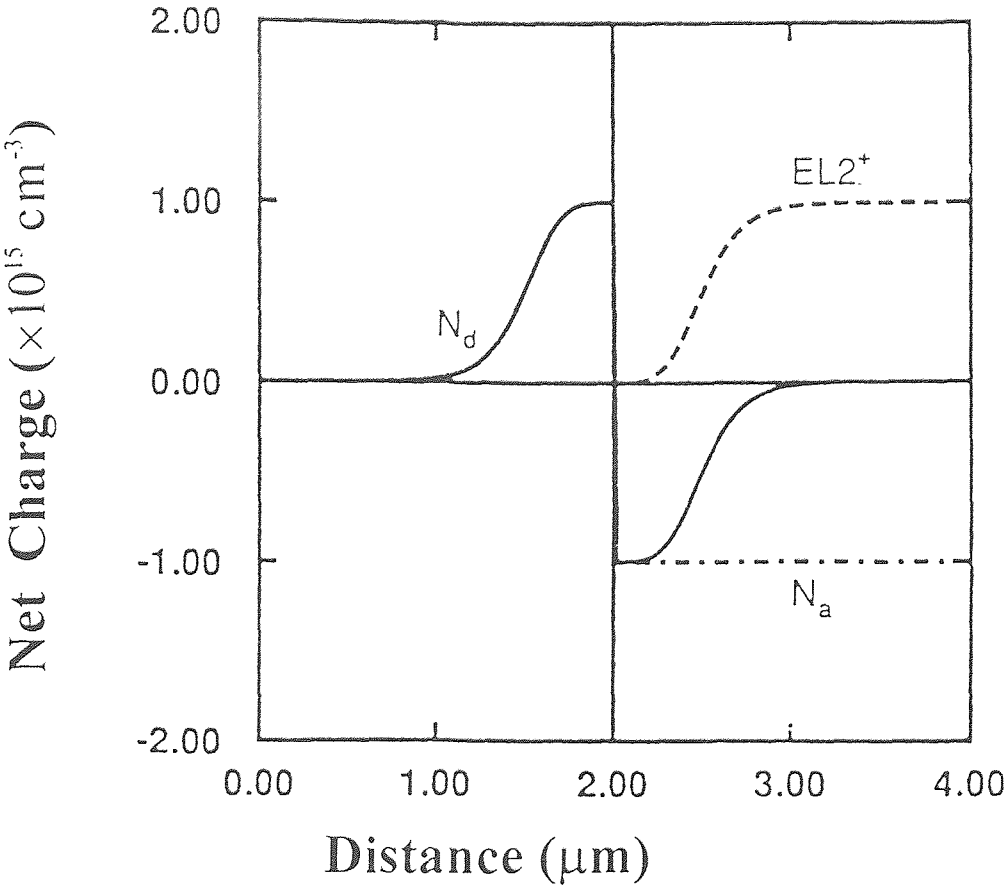

Figure 3.3 Comparison of the net charge distribution between the n-SI junction and the equivalent forward-biased n-p junction. The solid line represents the net charges. The dashed line and dot-dashed line are the ionized deep donor and shallow acceptor concentrations in the SI-layer separately.

By using the abrupt junction approximation, the space charge region width both in the semi-insulating layer (W_{di}) and n-type region (W_{dn}) are related to built-in potential (V_{bi}) by

$$W_{di} = \left[\frac{2\varepsilon}{qN_d}\,\frac{N_d}{N_a + N_d}\,V_{bi}\right]^{1/2} \tag{3.6}$$

$$W_{dn} = \left[\frac{2\varepsilon}{q\,N_d}\,\frac{N_d}{N_a + N_d}\,V_{bi}\right]^{1/2} \tag{3.7}$$

CHAPTER 4

DERIVATION OF ANALYTICAL MODELS FOR MESFET's IN THE SUBTHRESHOLD REGION

4.1 Charge Densities

By utilizing the concepts of previous chapters, we can proceed to derive analytical expressions. Consider the one-dimensional Poison equation along the axis normal to the gate. Refer to Fig. 4.1. By including the exponential terms representing mobile majority carriers in the channel and substrate, we have

$$\rho = q N_d \left[1 - \exp\left\{\frac{q[\psi - (V_{bi} + \phi_{ci})]}{KT}\right\}\right] \tag{4.1}$$

in the n channel active region, and

$$\rho = -q\left[N_a + N_d \exp\left\{\frac{q[\psi - (V_{bi} + \phi_{ci})]}{KT}\right\}\right] \tag{4.2}$$

in the semi-insulating region. Where ρ is net charge density, ψ the residual potential, ϕ_{ci} is the electron quasi-Fermi level referenced to the Fermi level in the neutral bulk substrate, V_{bi} the built-in potential of the substrate-channel junction, N_a is the substrate shallow acceptor concentration and Nd the channel doping concentration. All potentials are referenced to the neutral bulk substrate.

4.2 Areal Charge Densities

Referring to Figure 4.2. we can solve the Poisson equation in three regions, respectively.

1) Channel depleted region in the Schottky junction side

Begin with Poison equation, we have

$$\frac{dE}{dx} = -E\frac{dE}{d\psi} = \frac{\rho}{\varepsilon} \tag{4.3}$$

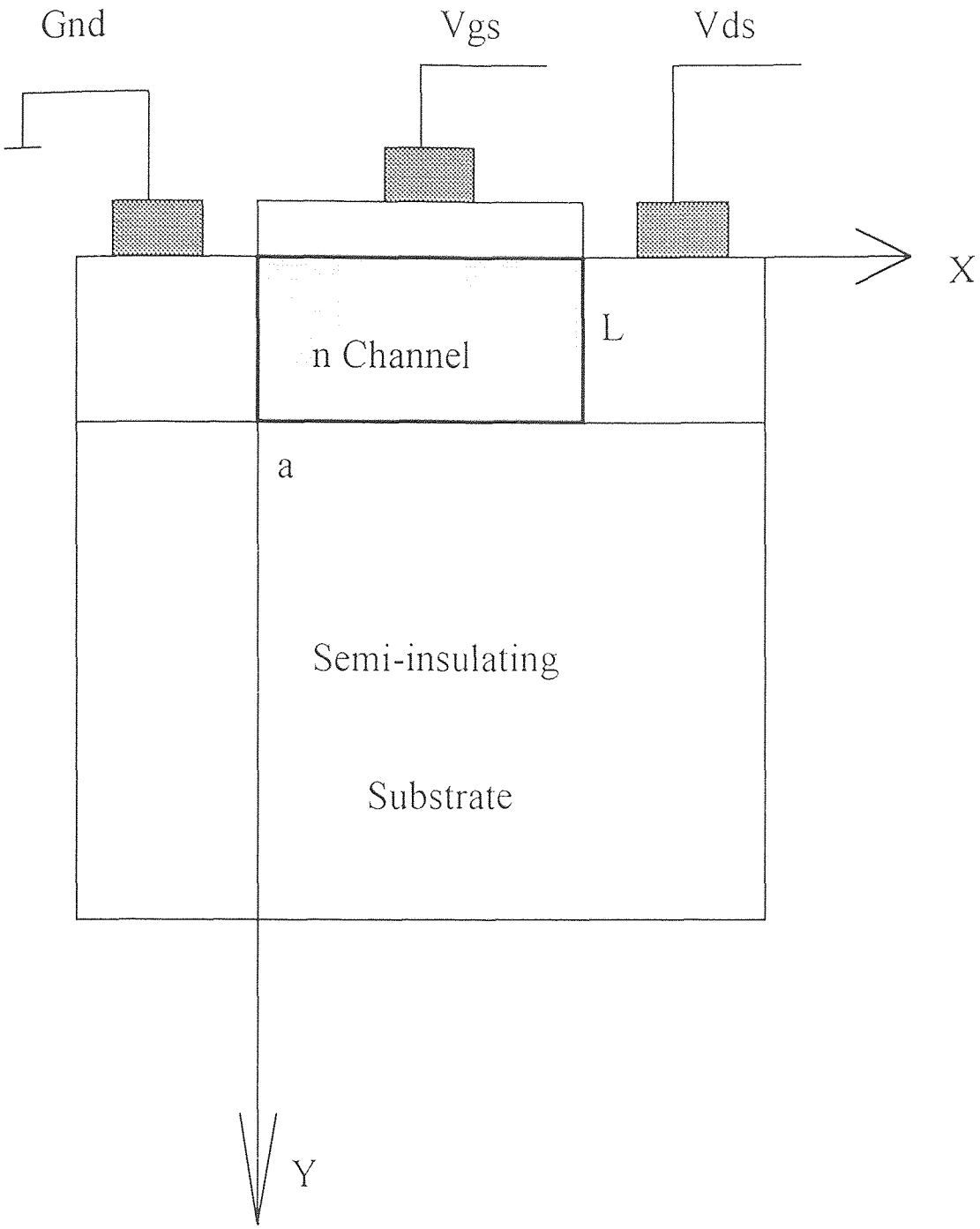

Figure 4.1 Cross section of a self-aligned gate MESFET. Poisson equation is along the y axis at an arbitrary position along the x axis.

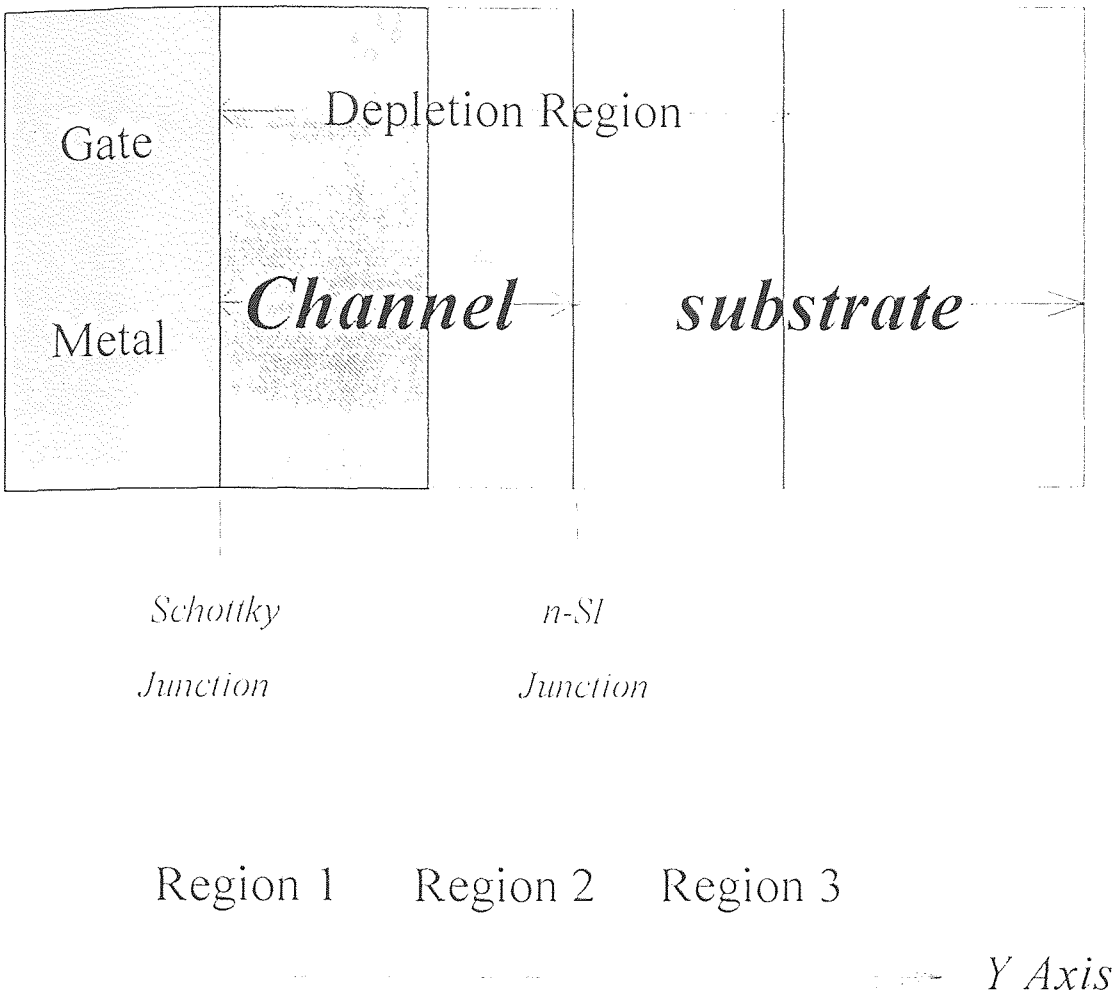

Figure 4.2 The calculated domain of gate-channel-substrate structure

Substituting for ρ from (4.1), we have

$$\int_0^{E_s} - e\,E\,dE = \int_{\psi_{cc}}^{\psi_s} q\,N_d\left[1 - \exp\left\{\frac{q[\psi - (V_{bi} + \phi_{ci})]}{kT}\right\}\right] d\psi \qquad (4.4)$$

or

$$-e E_s^2 = 2q N_d \{\psi_s - \psi_{cc} + \frac{kT}{q} \exp[-\frac{q}{kT}(V_{bi} + \psi_{ci})][\exp(\frac{q\psi_{cc}}{kT}) - \exp(\frac{q\psi_s}{kT})]\} \quad (4.5)$$

Where ψ_{cc} is the channel potential maximum between the gate and the substrate, ψ_s the surface (gate-channel interface) potential, E_s the surface potential.

Then using Gauss's law to assume that the electric field at the metal-semiconductor interface supports the charges on the gate side, the areal density of the charge on the gate side in the channel Q_{cg} is obtained as

$$Q_{cg} = [2e\, qN_d \{\psi_{cc} - \psi_s + \frac{kT}{q} \exp[-\frac{q(V_{bi} + \psi_{ci})}{kT}][\exp(\frac{q\psi_s}{kT}) - \exp(\frac{q\psi_{cc}}{kT})]\}]^{1/2} \quad (4.6)$$

2) Channel depleted region on the n-SI junction side

The derivation of the areal density of the charge in region 2 is done in the same manner as for region 1, and the areal charge density Q_{cn} is obtained as

$$Q_{cn} = [2\varepsilon q N_d \{\psi_{cc} - \psi_i + \frac{kT}{q} \exp[-\frac{q(V_{bi} + \psi_{ci})}{kT}][\exp(\frac{q\psi_i}{kT}) - \exp(\frac{q\psi_{cc}}{kT})]\}]^{1/2} \quad (4.7)$$

Where ψ_i is the potential at n-SI interface.

3) Semi-insulating region

Performing a similar derivation as above, we can get the expression for areal charge density in the semi-insulating region Q_{in}. This yields

$$Q_{in} = -\{2q\varepsilon N_a \psi_i + 2q\varepsilon N_d \frac{kT}{q} \exp[-\frac{q(V_{bi} + \psi_{ci})}{kT}][\exp(\frac{q\psi_i}{kT}) - 1]\}^{1/2} \quad (4.8)$$

Assuming that charges on opposite sides of the substrate-channel n-SI junction balance, we have

$$Q_{cn} = - Q_{in} \quad (4.9)$$

or

$$2q\varepsilon N_d\{\psi_{cc} - \psi_i + \frac{kT}{q}\exp[-\frac{q(V_{bi} - \psi_{ci})}{kT}][\exp(\frac{q\psi_i}{kT}) - \exp(\frac{q\psi_{cc}}{kT})]\}$$

$$= 2q\varepsilon N_a\psi_i + 2q\varepsilon N_d\frac{kT}{q}\exp[-\frac{q(V_{bi} + \psi_{ci})}{kT}][\exp(\frac{q\psi_i}{kT}) - 1] \tag{4.10}$$

Since $\psi_{cc} \leq V_{bi} + \psi_{ci}$, assuming ψ_{cc}, $\psi_i >> KT/q$, then

$$\psi_i \approx \frac{N_d}{N_d + N_a}\psi_{cc} = \gamma\psi_{cc} \tag{4.11}$$

Where

$$\gamma = \frac{N_d}{N_d + N_a} \tag{4.12}$$

Substitute (4.12) into (4.7) and (4.8), we have

$$Q_{cn} = [2q\varepsilon N_d\{\frac{N_a}{N_a + N_d}\psi_{cc} + \frac{kT}{q}\exp[-\frac{q(V_{bi} + \psi_{ci})}{kT}][\exp(\frac{q\gamma\psi_{cc}}{kT}) - \exp(\frac{q\psi_{cc}}{kT})]\}]^{1/2} \tag{4.13}$$

$$Q_{in} = -\{2q\varepsilon N_a\gamma\psi_{cc} + 2q\varepsilon N_d\frac{kT}{q}\exp[-\frac{q(V_{bi} + \psi_{ci})}{kT}][\exp(\frac{q\gamma\psi_{cc}}{kT}) - 1]\}^{1/2} \tag{4.14}$$

4.3 Mobile Charge Density

By applying Kirchoff's voltage law from the gate to the substrate, a relationship between the surface potential and the gate bias Vgs is obtained as

$$V_{gs} = \psi_{ms} - V_{bi} + \psi_s + V_{is} \tag{4.15}$$

where ψ_{ms} is the metal n-channel work function difference and Vis is the substrate bias. Furthermore, the sum total of the areal densities of the fixed charge and mobile carriers Qn in the channel is given by

$$q N_d a - q N_a W_{di} = Q_{cg} + Q_{cn} + Q_{in} + Q_n \tag{4.16}$$

where a is the channel thickness. In the subthreshold region, the channel and semi-insulating substrate are virtually depleted of mobile carriers. Then, neglecting the mobile carrier terms in (4.6), (4.13), (4.14), and using (4.15), the expression describing the variation of the channel potential with the gate bias in the subthreshold region is obtained as

$$V_{gs} = V_{ts} + (1 + \frac{C_{ci}}{C_{gc}})(\psi_{cc} - V_{bi} - \psi_{ci}) \tag{4.17}$$

where

$$V_{ts} = \psi_{ms} + (\psi_{ci} + V_{is}) - \frac{qN_d}{2\varepsilon}(a - W_{dn})^2 \tag{4.18}$$

$$C_{ci} = \frac{\varepsilon}{W_{dn} + W_{di}} \tag{4.19}$$

$$C_{gc} = \frac{\varepsilon}{a - W_{dn}} \tag{4.20}$$

$$W_{dn} = [\frac{2\varepsilon}{qN_a}\frac{N_a}{N_a + N_d}(V_{bi} + V_{ci})]^{1/2} \tag{4.21}$$

$$W_{di} = [\frac{2\varepsilon}{qN_a}\frac{N_d}{N_a + N_d}(V_{bi} + V_{ci})]^{1/2} \tag{4.22}$$

where C_{ci} is the substrate-channel depletion capacitance/area, C_{gc} is the gate-channel depletion capacitance/area, V_t is the threshold voltage, and W_{dn} and W_{di} are the depletion region widths on the n and SI sides, respectively.

The threshold condition at some arbitrary point between the source and the drain is said to occur when, at some point in the channel, the volume density of mobile carriers equals the background doping concentration. This is implies that, at threshold voltage $\psi_{cc} = V_{bi} + \psi_{ci}$. From (4.17), then, it follows that $V_{ts}$is the threshold voltage and that when $V_{gs} < V_{ts}$, that is, in the subthreshold region , $\psi_{cc} < V_{bi} + \psi_{ci}$. Since the channel is virtually depleted in the subthreshold region, the expressions for Q_{cg}, Q_{cn} and Q_{in} in (4.6) , (4.13) and (4.14) are expanded in Taylor's series about the exponential terms representing mobile carriers. Using the resulting expressions with (4.16), we have

$$Q_n = Q_{cg} + Q_{cn} - Q_{in} - q N_d a + q N_a W_{d1}$$

$$= \{2q\varepsilon N_d [(a-W_{dn}) \frac{qN_d}{2\varepsilon} - (V_{gs} - V_t) \frac{C_{ci}}{C_{gc}+C_{ci}} + \frac{kT}{q} \exp[\frac{q(V_{gs} - V_t)}{kT}]$$

$$- \frac{q^2 Nd}{2\varepsilon kT} (a-W_{dn})^2]] - \frac{kT}{q} \exp[\frac{q(V_{gs} - V_t)}{MkT}]\}^{1/2} +$$

$$+ \{2q\varepsilon N_d [(1-\gamma)(V_{bi}+V_{ci}) + (1-\gamma)(\frac{V_{gs}-V_t}{M}) -$$

$$\frac{kT}{q}(1-\gamma)\psi_{cc} \frac{q}{kT} \exp[\frac{q(V_{gs}-V_t)}{MkT}]]\}^{1/2}$$

$$- \{2q\varepsilon N_d [(1-\gamma)(V_{bi}+V_{ci}) + (1-\gamma)(\frac{V_{gs}-V_t}{M}) -$$

$$- \frac{kT}{q}(1-\gamma)\psi_{cc} \frac{q}{kT} \exp[\frac{q(V_{gs}-V_t)}{M}] +$$

$$+ \frac{kT}{q} \exp[\frac{q(V_{gs}-V_t)}{MkT}]]\}^{1/2} - q N_d a + q N_a W_{d1}$$

$$= q N_d (a - W_{dn}) - \frac{(V_{gs} - V_t)(M-1)}{M} C_{gc} - \frac{kT}{q} C_{gc} \exp\left[\frac{q(V_{gs} - V_t)}{MkT}\right] +$$

$$+ q N_d W_{dn} + C_{ci} \frac{V_{gs} - V_t}{M} - C_{ci} \psi_{cc} \exp\left[\frac{q(V_{gs} - V_t)}{MkT}\right] +$$

$$+ \left[C_{ci} \psi_{cc} - \frac{KT}{q} \frac{C_{ci}}{(1-\gamma)}\right] \exp \frac{q(V_{gs} - V_t)}{MkT} - q N_d a$$

$$= - \frac{kT}{q} \left(C_{gc} + \frac{C_{ci}}{1-\gamma}\right) \exp\left[\frac{q(V_{gs} - V_t)}{MkT}\right] \tag{4.23}$$

where $M = 1 + \frac{C_{ci}}{C_{gc}}$.

4.4 Subthreshold Drain Current

The subthreshold drain current - voltage characteristics of a MESFET are derived by using (4.23) in the following relation for the drain current Ids prescribed by the classical gradual channel analysis.

$$I_{ds} = \frac{W}{L} \overline{\mu_n} \int_{-V_{is}}^{V_{ds} - V_{is}} Q_n(\psi_{ci})\, d\psi_{ci} \tag{4.24}$$

where W is the width of the channel, L the length of the channel and $\overline{\mu_n}$ the average channel electron mobility. The characteristic equation in the subthreshold region of operation, thus obtained, is presented below:

$$I_{ds} = \frac{W}{L} \overline{\mu_n} C_{gc0} \left[1 + \frac{C_{ci0}}{(1-\gamma) C_{gc0}}\right] M_0 \left(\frac{kT}{q}\right)^2 \exp\left[\frac{q(V_{gs} - V_{t0})}{M_0 kT}\right] \tag{4.25}$$

where M_0, V_{t0}, C_{gc0} and C_{ci0} are the corresponding quantities evaluated at $\psi_{ci} = -V_{is}$.

The equation (4.25) is similar in form to the empirical subthreshold current equation [see equation (4.26) below] offered by Conger et al [8] which very accurately describes the observed dependence of subthreshold current on Vgs and Vt.

$$I_{dsub} = I_{so} \exp[\frac{q(V_{gs} - V_t)}{MkT}] \tag{4.26}$$

Where Iso is the threshold leakage current. In equation (4.25), it can be expressed as

$$I_{so} = \frac{W}{L} \overline{\mu_n} C_{gc0} [\, 1 + \frac{C_{ci0}}{(1-\gamma)C_{gc0}} \,] M_0 (\frac{kT}{q})^2 \tag{4.27}$$

CHAPTER 5

RESULTS AND DISCUSSION

5.1 Comparison of Analytical Model and Empirical Model

Equations (4.25) and (4.26) are compared for an enhancement-mode MESFET and a depletion-mode MESFET, respectively. Table 1 shows the comparison. The experimental results were based on (4.26) where the subthreshold parameters were those extracted from a least-squares fitting program. The analytical results were based on (4.25). $\overline{\mu_n}$ was evaluated by the calculation of channel electric field intensity in the subthreshold region and using equation (2.10). The agreement between the measured and calculated results is good.

Table 1 The comparison of experimental and analytical results

Device Type	Device Parameters	Method	Iso	Mo
Device 1 Enhancement MESFET	W=20 u L=1 u Vt = .103 V	Measured Value	7.69 uA	1.30
		Calculated Value	7.55 uA	1.28
Device 2 Depletion MESFET	W=14 u L = 1 u Vt = -0.74 v	Measured Value	2.46 uA	1.35
		Caculated Value	2.55 uA	1.355

5.2 Subthreshold Swing

Figure 5.1 shows the practical drain current, Id, versus gate voltage, Vgs. It is easily seen that the subthreshold drain currents varied exponentially (i.e. , linear in a semi-logarithmic plot) in the region of subthreshold. This exponential behavior was predicted by equations (4.25) and (4.26).

In equation (4.25), we know the subthreshold slope factor $M_o = 1 + \frac{C_{ci\,o}}{C_{gco}}$, which gives us a single expression for the subthreshold swing S

$$S = \frac{\partial V_{gs}}{\partial \log I_{ds}} = \frac{\frac{kT}{q} \ln 10}{M_o} \tag{5.1}$$

5.3 Device Parameter Dependence on Subthreshold Characteristics

Our analytical model is used to investigate the influences of device parameters on the subthreshold characteristics of MESFET's with undoped substrates. In this section the subthreshold factor, Mo, and threshold leakage current, Iso, are plotted as functions of the device threshold voltage (Vt), residual acceptor concentration (Na), deep level EL2 concentration (Nt) and channel doping (Nd).

Figure 5.2 and Figure 5.3 show Mo and Iso versus residual shallow acceptor concentration Na with threshold voltage Vt=.1,-.3 and -.7 V. It is seen that as Na increases, Mo increases but Iso decreases. All the two curves are similarly characterized by a rapidly varying region followed by a slow increasing or decreasing region. At high shallow acceptor concentration , Mo(Na) and Iso(Na) curves have an almost linear dependence. Below some concentration, the two parameters vary sharply. For example, in the region shown in figure 5.2, subthreshold factor Mo increases about 30 % when the shallow acceptor

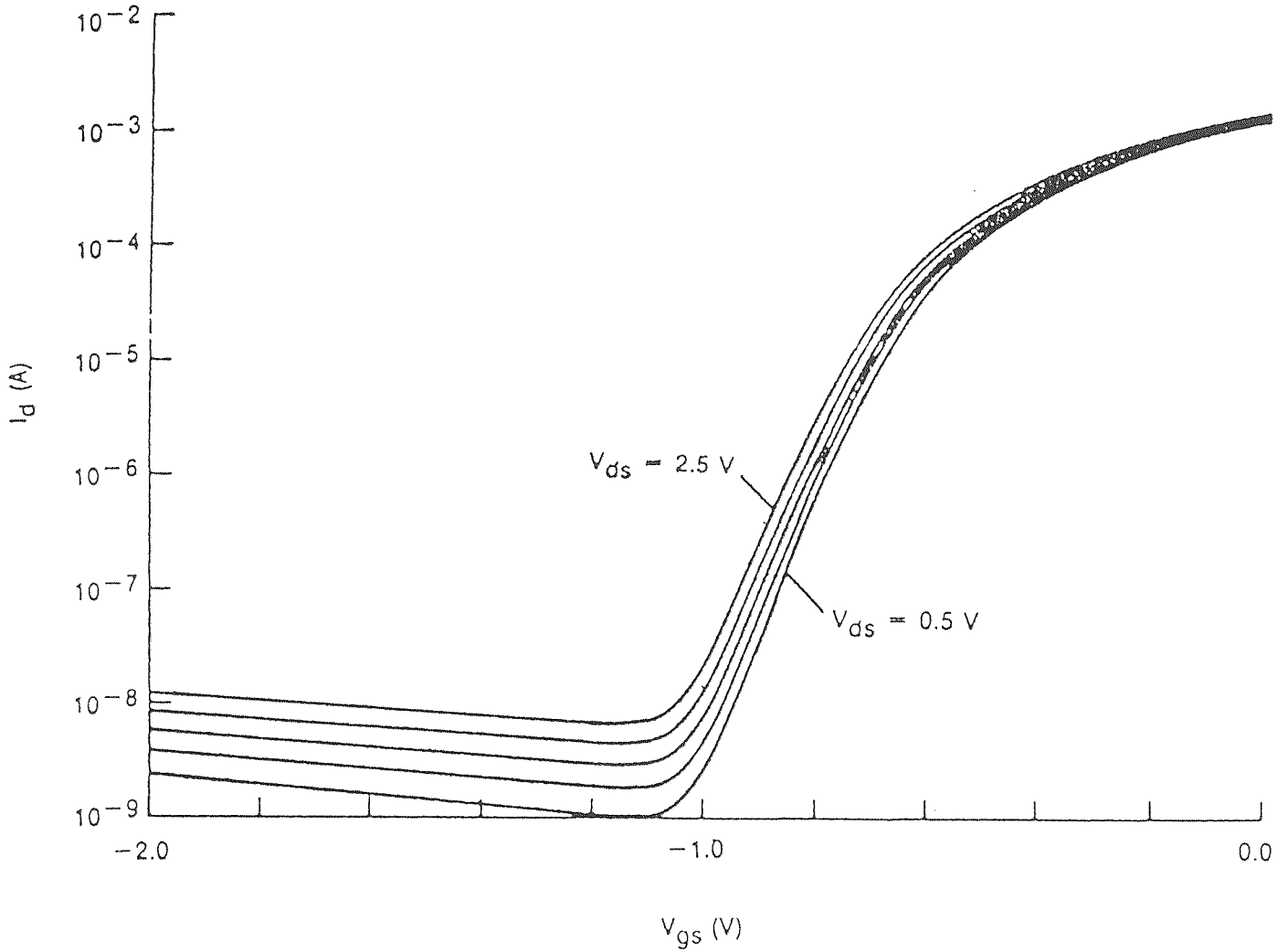

Figure 5.1 Subthreshold characteristics of GaAs MESFET's

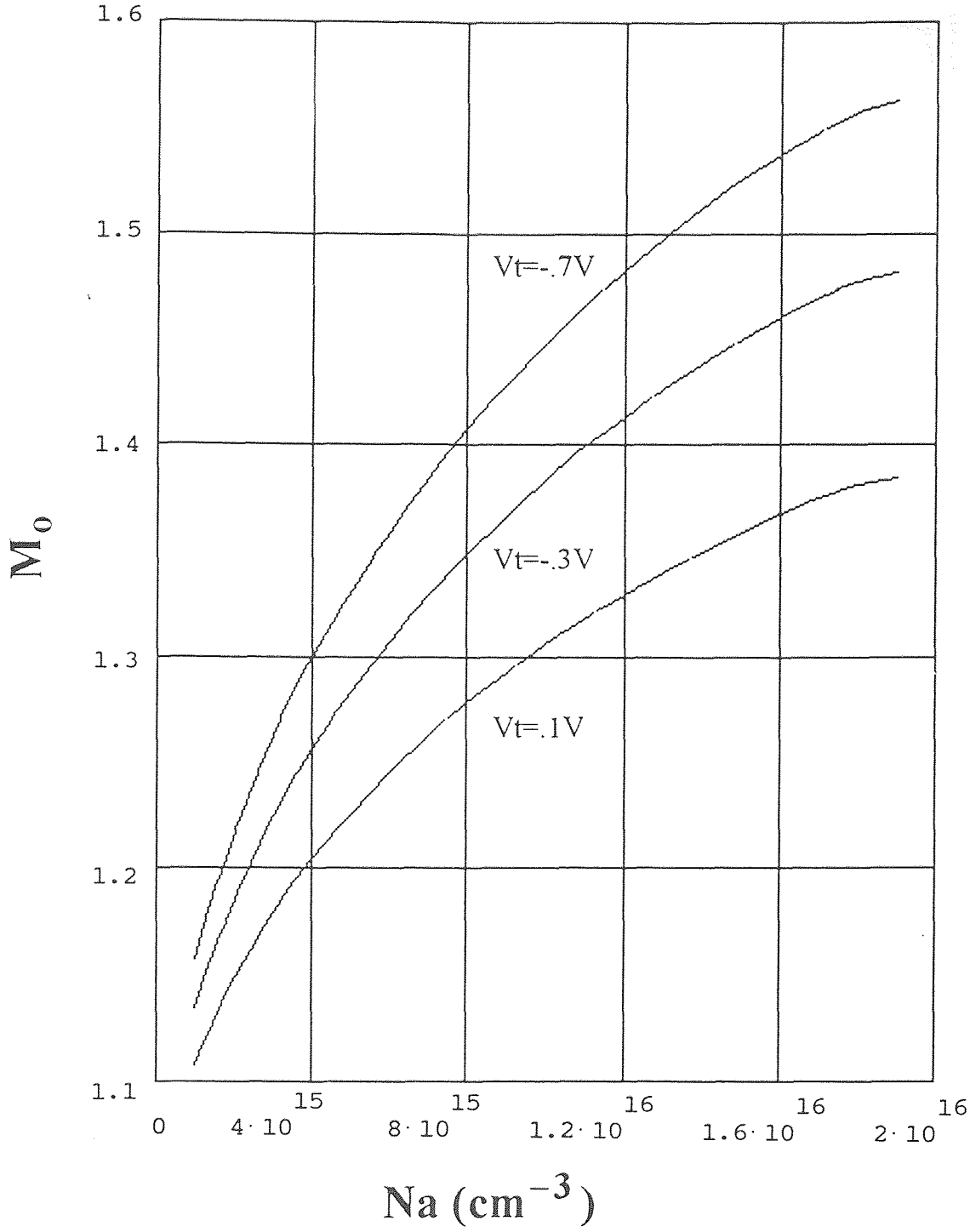

Figure 5.2 Subthreshold factor Mo plotted as a function of residual acceptor concentration Na (cm^{-3}) and threshold voltage Vt

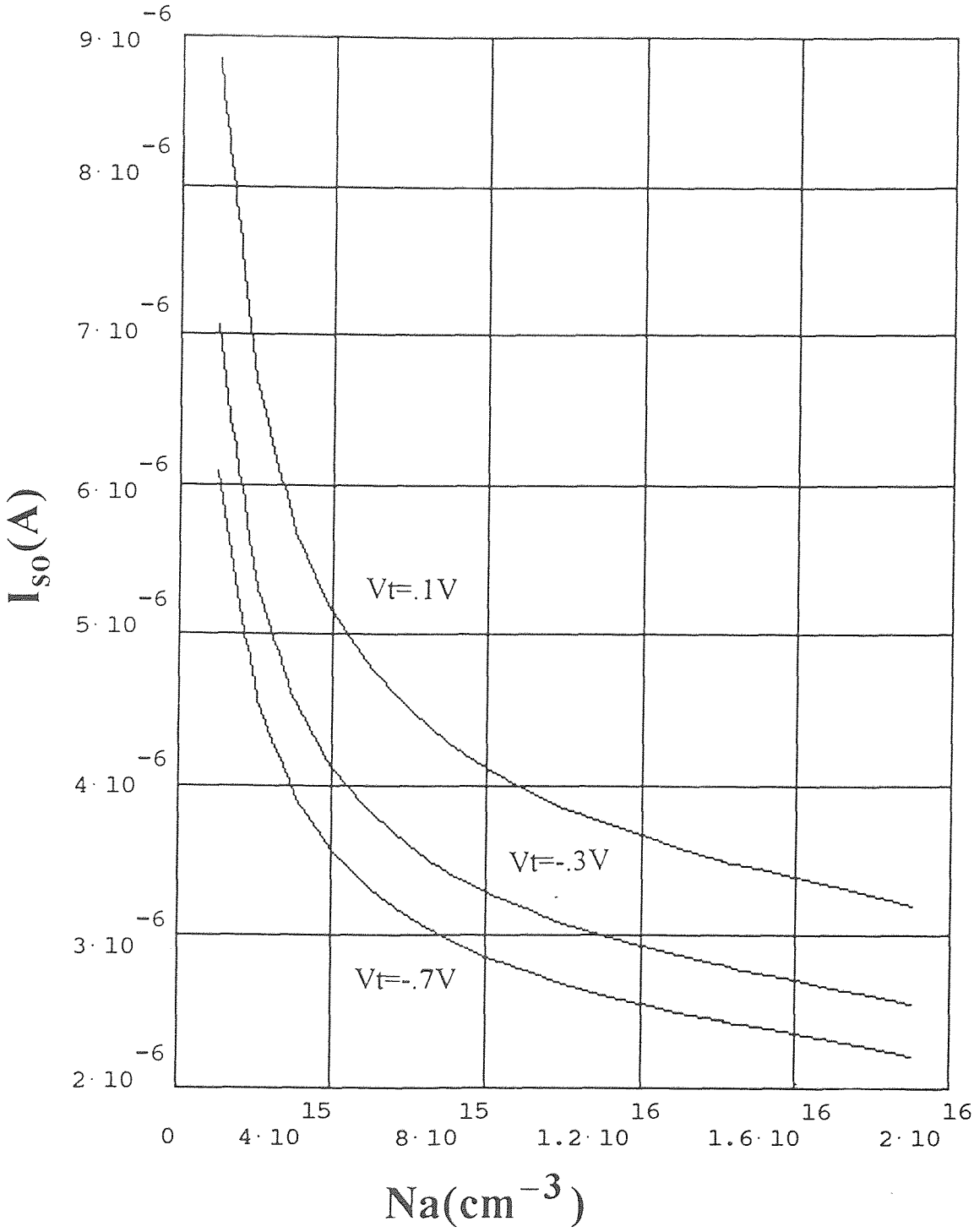

Figure 5.3 Threshold leakage current Iso (A) plotted as a function of residual acceptor concentration Na (cm^{-3}) and threshold voltage (V).

concentration Na increases by one order of magnitude. These results are due to an decrease in depletion width of the channel substrate junction.

Figure 5.4 and Figure 5.5 demonstrate the calculated Mo(Nt) and Iso(Nt) characteristics with different threshold voltage. In the calculation, the residual acceptor concentration Na is assumed to have a value of $1\times10^{15}\mathrm{cm}^{-3}$ and the channel doping concentration Nd is assumed to have a value of $1\times10^{17}cm^{-3}$. These values correspond to typical values found in MESFET's. It is clear from the figures that the Mo and Iso both increase as the deep level concentration Nt increases . Over the Nt region studied , the variations of Mo and Iso are very limited and are much smaller than those for Na dependence in Figure 5.2 and Figure 5.3 correspondingly. This can be easily understood since according to our model, Nt is only related to ψ_{bi} which can be changed in a very limited region. So the deep level concentration dependence on subthreshold characteristics is relatively weak as compared to other parameter dependencies.

The subthreshold factor Mo decreases as the channel doping concentration Nd is increased, as seen in Figure 5.6. In this figure the decrease is more significant for smaller threshold voltage. This effect can be used to optimize the subthreshold characteristics in conventional processing of GaAs MESFET's since, in general , we cannot change the residual acceptor concentration for a given GaAs wafer, but we can easily adjust the channel doping concentration during processing.

Figure 5.7 shows the Iso variation with channel doping concentration. This figure has a special feature which is different from previous figures. The curves in this figure consist of two regions; region -1 and region-2 . In region-1 at lower Nd values, the current decreases with channel doping concentration. In region-2 at higher Nd values , the current increases nearly linearly with channel doping concentration. There exists a minimum Iso value for each threshold voltage. The

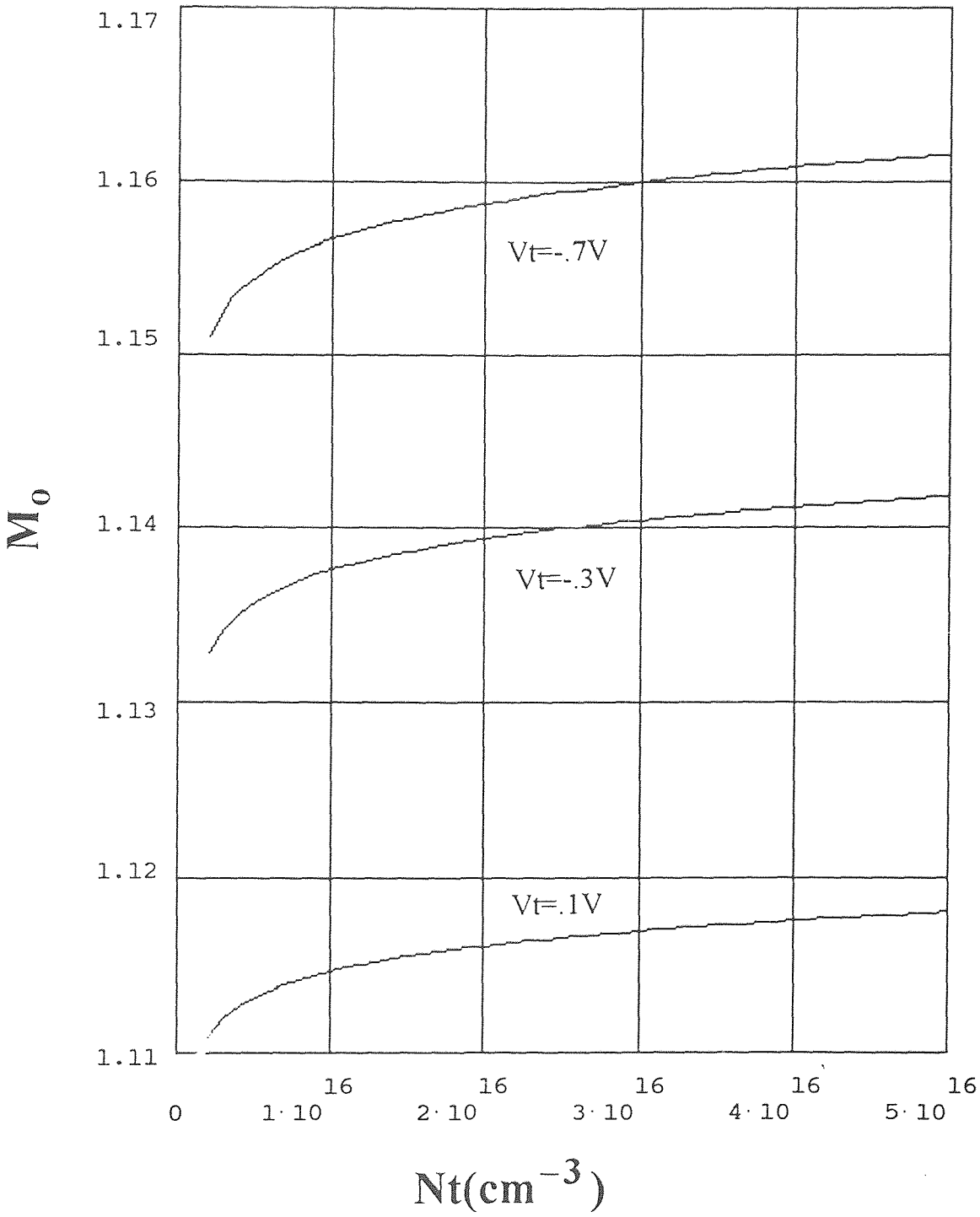

Figure 5.4 Subthreshold factor Mo calculated as a function of deep level EL2 concentration Nt (cm^{-3}) and threshold voltage

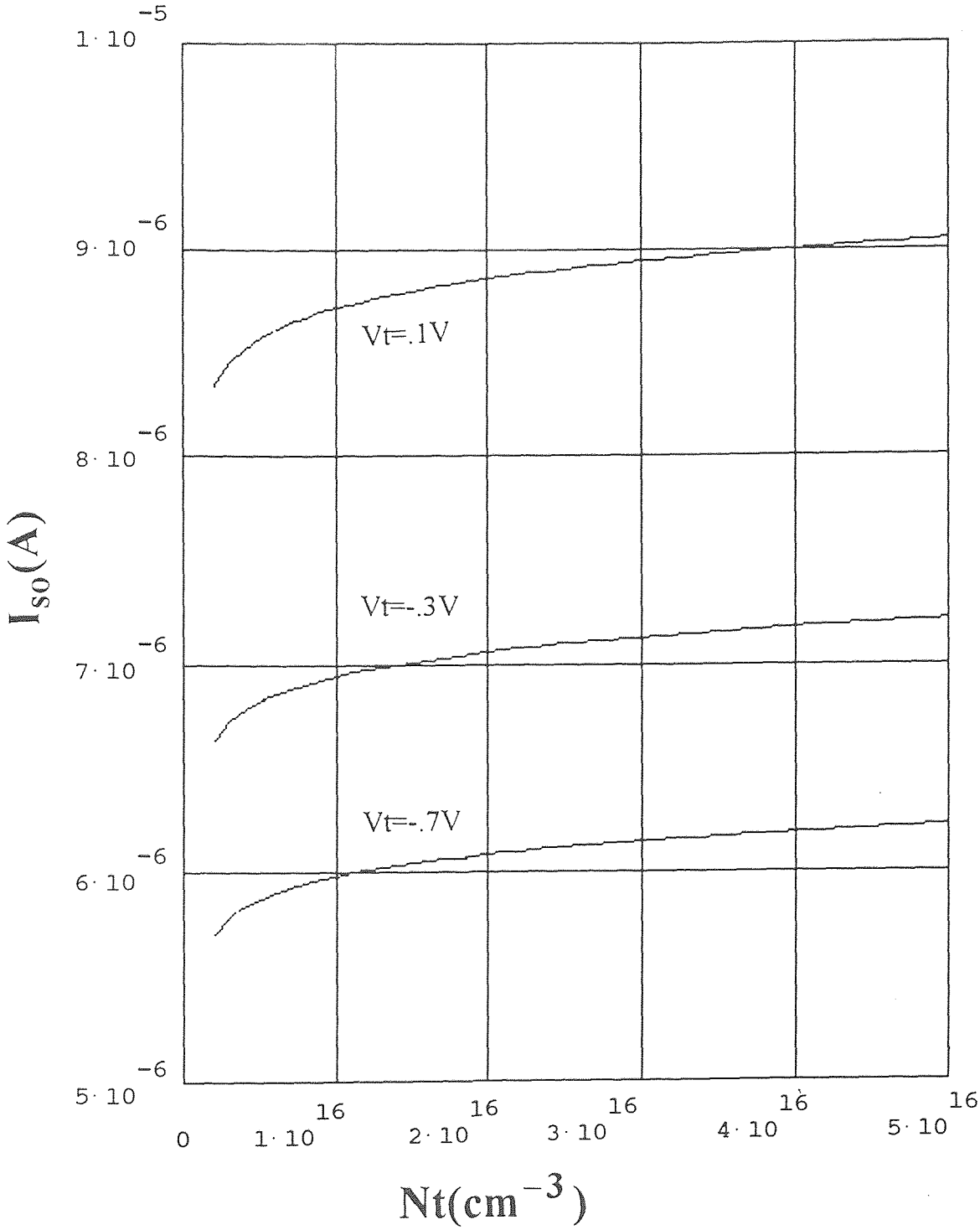

Figure 5.5 Threshold leakage current Iso (A) calculated as a function of deep level concentration Nt (cm^{-3}) and threshold voltage Vt

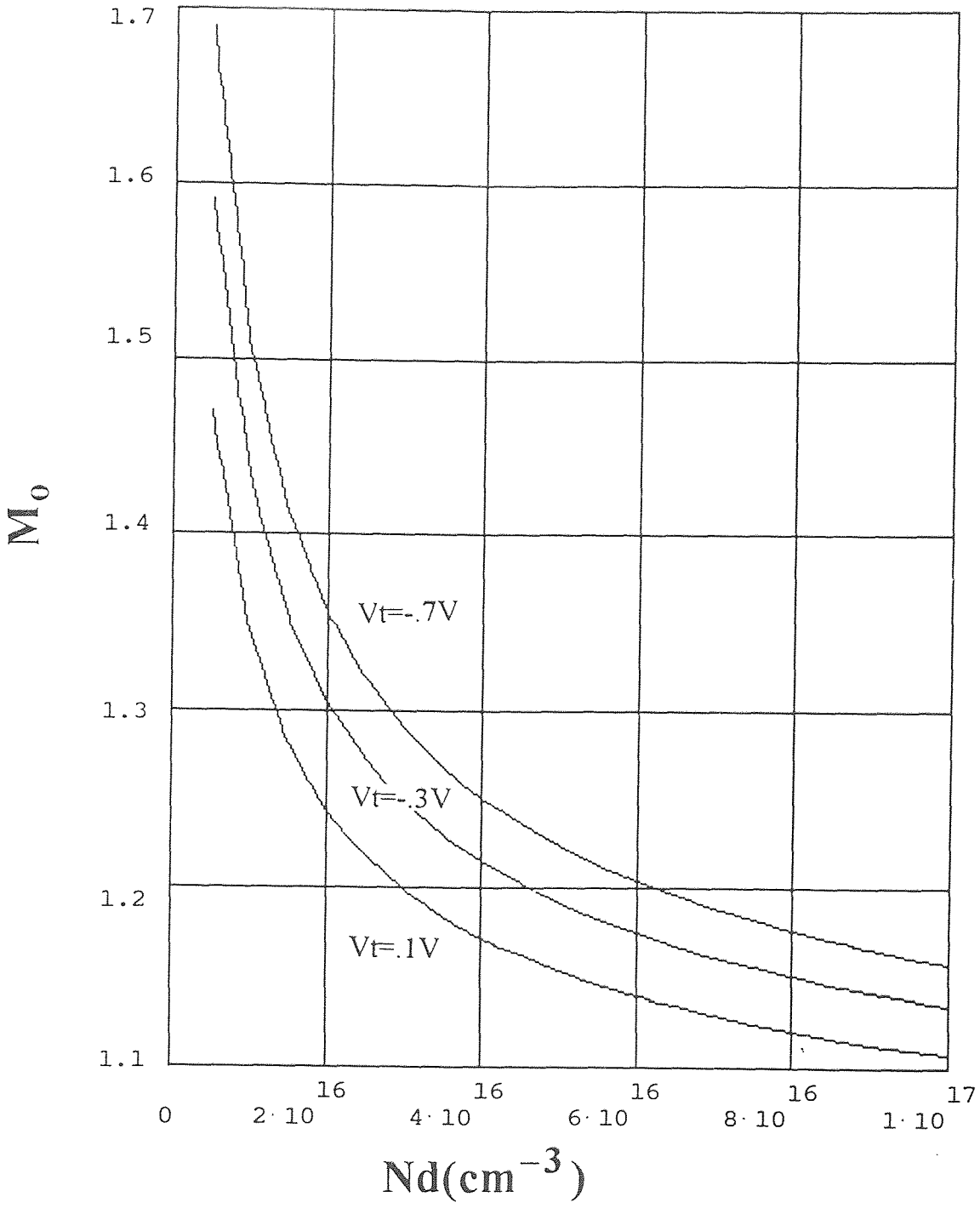

Figure 5.6 Subthreshold factor Mo calculated as a function of channel doping concentration Nd (cm^{-3}) and threshold voltage Vt (V).

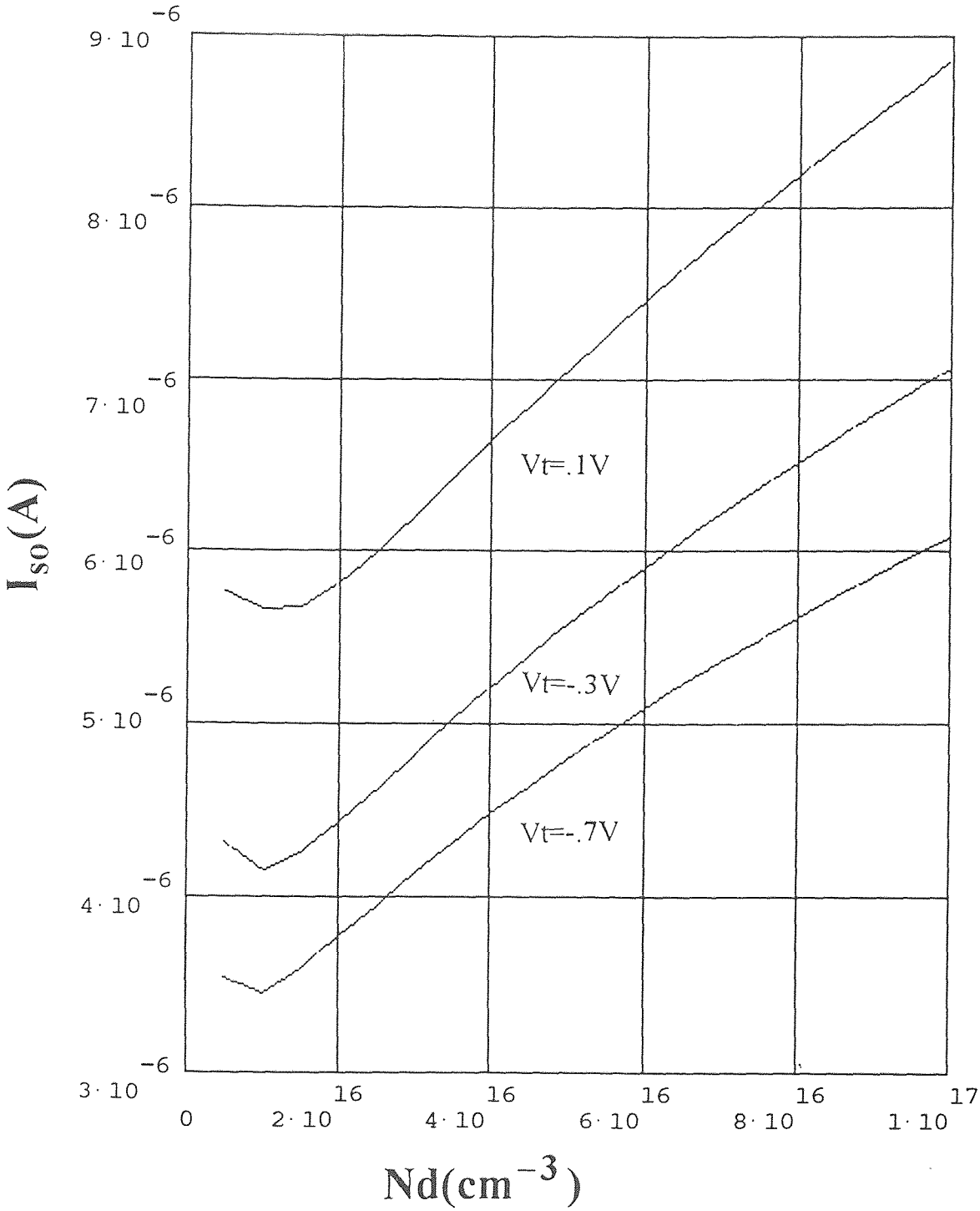

Figure 5.7 Threshold leakage current Iso (A) plotted as a function of channel doping concentration Nd (cm^{-3}) and threshold voltage Vt (V)

Nd value corresponding to the minimum Iso is reduced as the threshold voltage decreases (becomes more negative).

As indicated in Figure 5.2, 5.4, and 5.6, the subthreshold factor Mo is reduced as the threshold voltage Vts is increased for given values of Nd, Na and Nt. We know from equation (5.1) that the subthreshold swing S is the reciprocal of the subthreshold factor. To obtain good subthreshold characteristics or smaller S values, since enhancement-mode MESFET's have larger threshold voltage than depletion-mode MESFET's, we should increase the threshold voltage alternatively, we could use enhancement MESFET's which have higher threshold voltage values . Also we can learn from Figures 5.2,5.4 and 5.6 that the subthreshold swing is most strongly dependent on the residual acceptor concentration in the semi-insulating substrate. For highly compensated SI substrate, the swing goes larger as the shallow acceptor concentration increases. Hence better subthreshold behavior will be expected for less compensated SI substrate.

Consider the threshold voltage dependence on threshold current Iso. It is seen from Figures 5.3, 5.5 and 5.7 that Iso increases as the threshold voltage Vts increases for the same other parameters studied. This is consistent with experimental results observed by Chang and Conger et al., [8][9] that enhancement-mode MESFET's have higher Iso than depletion-mode MESFET's.

5.4 Gate Leakage Current

A second feature of the GaAs MESFET subthreshold characteristics is the gradual increase in Ids after rapid initial drop beyond Vt (see the region of Vgs< -1 V in Figure 5.1). It was found that the major portion of Ids in this slowly rising region was caused by gate conduction through the reverse-biased gate-to-drain diode.

The solid curve in Figure 5.8 shows a reverse-biased I-V curve for a Schottky diode. In this case, the diode chosen is the gate-to-drain junction of the MESFET.

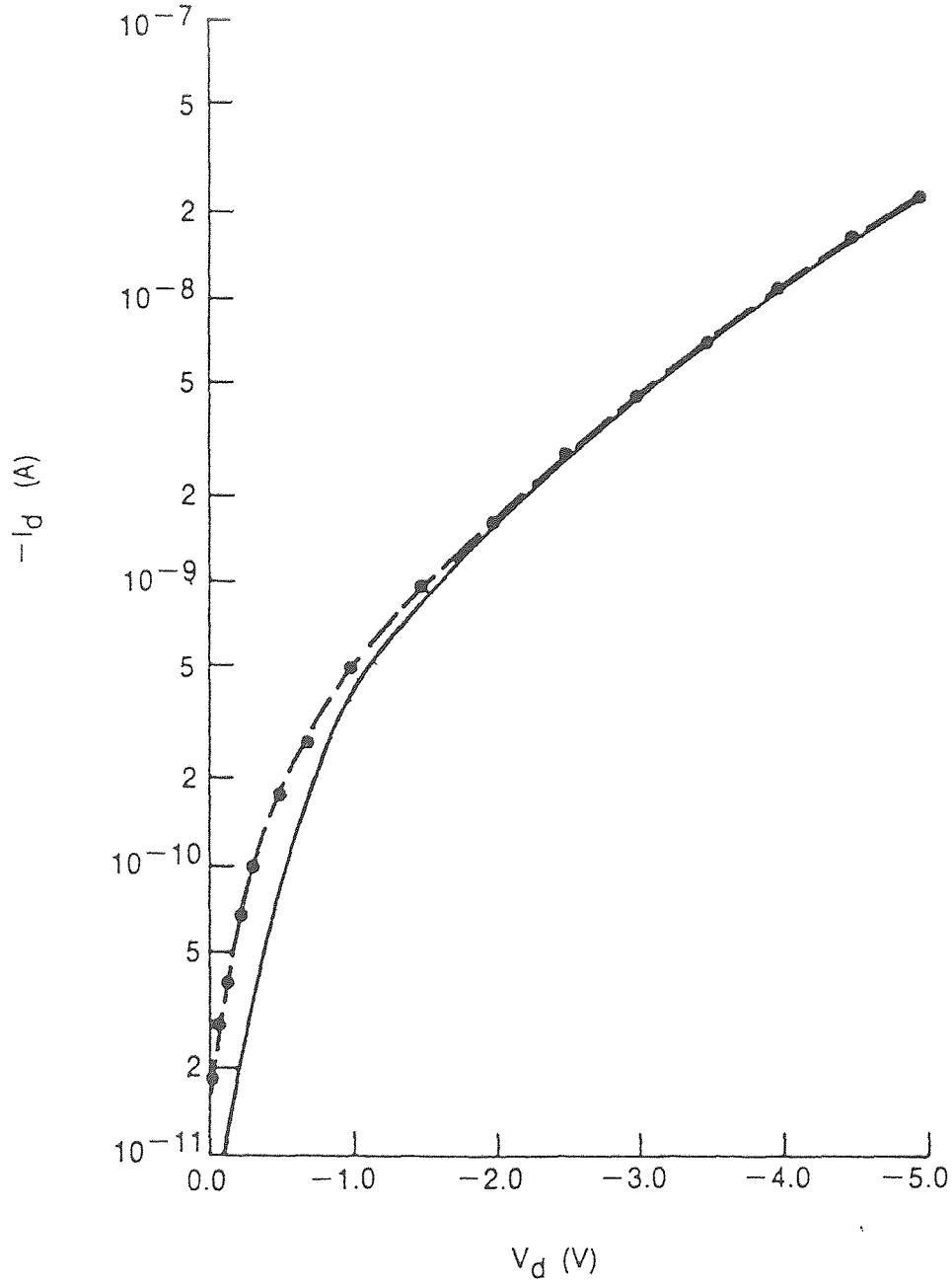

Figure 5.8 Comparison of measured (solid line) and calculated (solid circles on dashed line) Schottky-diode reverse-biased characteristics. Calculation is based on equation (5.2) as shown in next page.

The reverse diode current Id increases rapidly in the beginning, and increases monotonically with a smaller slope for large Vd . This is contrary to the behavior found in a classical diode (for example a silicon p-n junction diode), where the reverse current remains constant for reversed applied voltage Vd, until a catastrophic breakdown occurs. The slower increase in current for larger |Vd| can be easily understood since the Schottky barrier is lowered when it is reverse biased . In contract, a definite explanation for the rapid initial reverse current increase is more difficult. The change of slope in the I-V curve show in Figure 5.8 implies that there could be a change in the dominant conduction mechanism. The relatively small Schottky- barrier height and the comparatively large low-field electronic mobility in GaAs suggest that this may be caused by electronic tunneling.

A diode model was built to account for the reverse conduction of the gate-to-drain junction. The reverse diode current is described by an expression given by Dunn[10]:

$$I_d^{diode} = W\,L\,g_{ds}V_d \exp\left(-\frac{q\,V_d\,\delta}{KT}\right) \qquad (5.2)$$

for Vd<0 , where g_{ds} is the diode reverse conductance per unit area , and δ is a reverse-bias conduction parameter.

5.5 Subthreshold Characteristics

Equations (4.25) and (5.2) were implemented, and drain-current characteristics for a W/L= 14μ/1μ depletion-mode device were simulated for values of Vgs from -2.0 V to 0.0V. The threshold voltage Vt for this device was approximately -0.73 V. Figure 5.9 shows the simulated results and measured values. The agreement between the simulated and measured curves is very good.

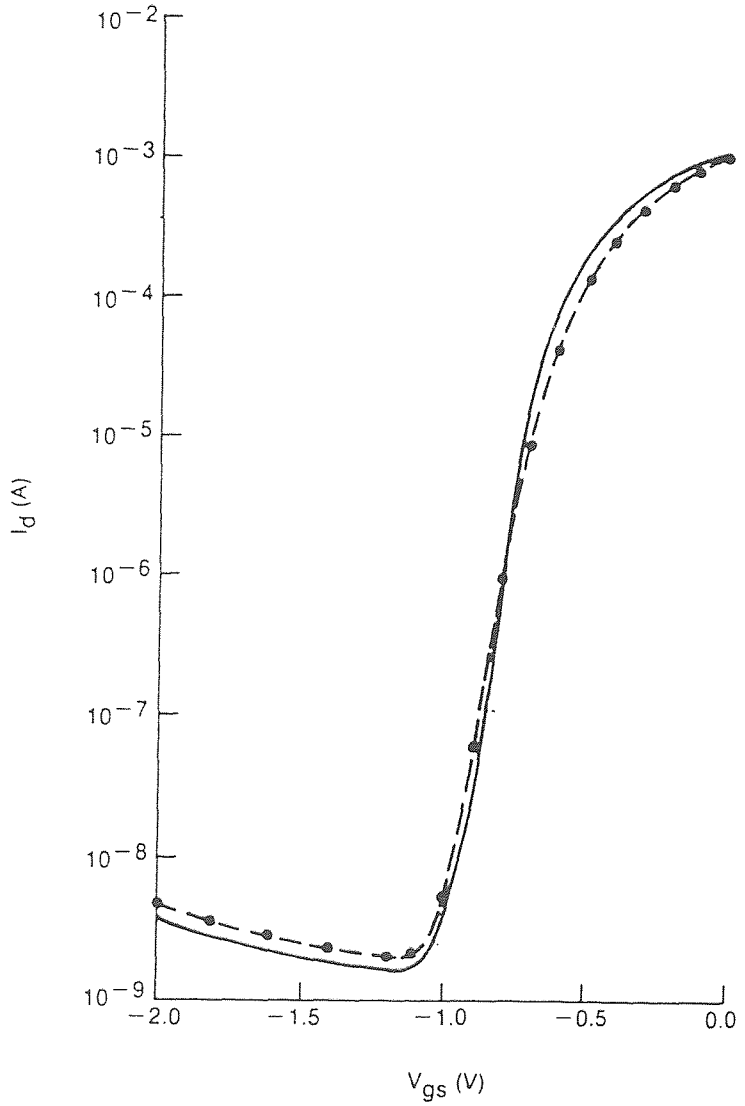

Figure 5.9 Comparison of measured (solid line) and calculated (solid circles on dashed line) voltage and current for a GaAs MESFET with W=14μm , L=1μm and Vt= −0.7 V. Calculation is based on the analytical model (equation (4.25)).

CHAPTER 6

DESIGN RULES AND CONCLUSION

6.1 Design Rules

The subthreshold characteristics for MESFET's with undoped substrates have been analyzed using an analytical model. It has been shown how the subthreshold leakage current depends on the device parameters. The derived simple analytical expressions is good for quick evaluation of the subthreshold swing and threshold leakage current for GaAs FET's with doped and undoped substrates. These analytical results can be used to develop the design rules for optimized subthreshould characteristics.

In designing MESFET's , we should first determine the best device geometric structures. It is clear from equation (4.25) that the smaller the gate width or the larger the gate length we design , the smaller the leakage current will be. But according to equation (5.2) , the reverse Schottly diode leakage current will increase if we choose larger gate lengths. So there must be some trade off in the geometric size design. For example the use of minimum sized FET's (i.e., let W=L=minimum allowed size).

Secondly, we must design the device physical parameter. There are three device parameters (Na, Nd and Vt) which strongly influence the subthreshold characteristics. Consider the shallow acceptor concentration first. From the analytical results we know that best result comes from less compensated substrates. So we should choose the lowest residual acceptor concentration wafer to do the processing. Alternatively, we could use undoped or very low doped MBE buffer layers (Carbon free) between the channel layer and semi-insulating substrate.

The other two parameters we should carefully design are the channel doping concentration and threshold voltage. According to results of this thesis, we should choose higher channel doping concentration and larger threshold voltage (more positive). Because the threshold voltage is related to channel thickness, highly doped shallow channel-substrate junctions are required.

In short , to get best subthreshold leakage characteristics , we should:

1) use minimum size FET's.

2) choose the lowest shallow acceptor concentration wafer, or
   use a low doped MBE buffer layer.

3) use enhancement FET's.

4) increase channel doping concentration.

6.2 Conclusion

In this thesis , a physical model for semi-insulating substrate including the substrate compensation properties is presented. The Poison equation is solved analytically in one dimension for GaAs MESFET's with undoped substrates in the subthreshold region. The solution is then used to derive expressions for subthreshold drain current and subshreshold swing in MESFET's with undoped substrates. Very good agreement between experimental and analytical results is achieved.

From the analytical results, it has been shown how the subthreshold characteristics depend on the compensation property of the substrate layer and device parameters. Two key parameters (Mo and Iso) that determine the subthreshold characteristics have been analyzed as functions of residual acceptor concentration Na , deep level EL2 concentration Nt, channel doping concentration Nt and threshold voltage Vt. It is shown that Mo increases with increasing Na and Nt, but decreases with increasing Nd and Vt . For Iso , the results show it increases

with increasing Nd, Nt and Vt , but decreases with increasing Na. The results also show that Nt has negligible effect on subthreshold characteristics . The subthreshold leakage current is most strongly influenced by Na, Nd and Vt. According to these results, useful design rules are presented for the design of devices with good subthreshold leakage characteristics.

In addition to providing expressions which are easy to evaluate, the analytical model presented in this thesis also gives us simple explanation for the observed subthreshold characteristics and offers a useful basis for accurate analysis, simulation and fabrication of GaAs FET's with ultra low leakage current. Although this analytical model is derived specially for GaAs MESFET's with undoped substrates , similar expressions can be derived for various III-V FET's which use leteroepitaxial structures.

REFERENCES

1. B. F. Levin, "Quantum-well infrared photodetectors," *J. Appl. Phys.*, Vol. 74, pp. R1-R81, Oct. 1993.

2. G. M. Martin, J. P. Farges, G. Jacob, J. P. Hallais, and G. Poibland, "The compensation mechanisms in GaAs," *J. Appl. Phys.*, Vol.51, pp. 2840-2852, June 1980.

3. W. Schockley and W.T. Read, "Statistics of the recombination of holes and electrons," *Phys. Rev.*, Vol.87, pp. 835-851, Dec. 1952.

4. V. Y. Prnz and S. N. Rechkunov, "Influence of a strong electric field on the carrier capture by nonradiative deep-level centers in GaAs," *Phys. Status solidi(B)*, Vol.118, pp. 159-166, Jan. 1983.

5. M. Hirose, J. Yoshida, and N. Toyada, "An improved two dimensional simulation model for GaAs MESFET applicable to LSI design." *IEEE Trans. Computer-Aided Des.*, Vol. 7, pp.225-230, Feb. 1988.

6. S. M. Sze, *Physics of Semiconductor Devices*, 2nd ed., New York, NY: Wiley, 1981.

7. D. E. Holmes, R. T. Chen, K. R. Elliot, C. G. Kirkpatrick, and P. W. Yu, "Compensated mechanism in liquid encapsulated Czochralski GaAs: importance of melt stoimetry," *IEEE Trans. Electron Devices*, Vol. 29, Sept. 1982.

8. J. Conger, A. Peczalski, and M. S. Shur, "Subthreshold current in GaAs MESFET's," *IEEE Electron Device Letters*, Vol. 9, pp.128-129, Mar. 1988.

9. C. T. Chang, T. Vrotsos, M. T. Frizzell, and R. Carroll, "A subthreshold current model for GaAs MESFET's," *IEEE Electron Device Letters*, Vol. 8, pp. 69-71, Feb. 1987.

10. C. Dunn, *The Microwave Semiconductor Devices and Their Circuit Applications*, New York, NY: McGraw-Hill, 1969.